PHYSICAL REVIEW D VOLUME 33, NUMBER 5 1 MARCH 1986

Transverse-momentum behavior of jets from generalized Altarelli-Parisi equations

L. M. Jones and L. Sagalovsky
Physics Department, University of Illinois, 1110 West Green St., Urbana, Illinois 61801

R. Migneron
Department of Applied Mathematics, University of Western Ontario, London, Ontario N6A 5B9 Canada
(Received 7 March 1985)

We present numerical solutions of previously reported integrodifferential equations for the transverse-momentum behavior of jets predicted by QCD. Results for the nonsinglet fragmentation functions of quarks are compared with approximate solutions in the literature obtained from other equations.

I. INTRODUCTION

One of the interfaces between QCD theory and experiment has been the transverse-momentum spread of jets. This is a jet property which is susceptible to measurement, and it is also something which can be predicted in various ways from the theory.

For instance, starting with the simplest perturbation-theory calculations, one can study the typical transverse-momentum distribution of hard gluons emitted from a quark using a QCD vertex.[1] The ϵ,δ definition of jet size, popularized by Sterman and Weinberg,[2] has been used to define jets; this is a method of specifying the transverse spread of each individual jet and defining the boundary between two-jet and three-jet events.

Another set of predictions in the literature, with attempts to check them experimentally, is obtained from the jet calculus of Konishi, Ukawa, and Veneziano[3] (KUV) and similar methods which sum infinite series of graphs.[4] In this case, leading-logarithmic perturbation theory is used to help predict the spread of angle between any two particles in the jet. Experimentalists have reported verifications[5] of the predictions, which help test the basic vertices in QCD.

Another thing one can do with the data is to define a jet axis somehow and measure the distribution of outgoing particles relative to this axis. This has been done by the TASSO group[6] and others,[7] with results plotted showing the average transverse momentum of jet particles as a function of their longitudinal momentum, and (summed over longitudinal momentum) the distributions of the data at various Q^2 as a function of $p_\perp$ and $x_T=2p_\perp/W$.

If one wishes to predict this from the theory, more needs to be done than in the KUV approach, where the opening angle between the two particles measured was defined in terms of the mass of the "parent parton" at that vertex. We need equations for the jet calculus which explicitly display both the transverse and the longitudinal momentum of the outgoing partons.

This was first done by Bassetto, Ciafaloni, and Marchesini[8] (BCM), who give an equation for the jet which generalizes the Altarelli-Parisi equations to take into account transverse momentum. Unfortunately, because in the Altarelli-Parisi approach the vertices are added at the large mass end of the jet, the jet axis keeps turning as more and more vertices are added. This means that in the BCM approach, the longitudinal and transverse momenta tend to be coupled. BCM, by using an ingenious trick, were able to obtain an approximate formula which should approach the correct answer as $x\to 1$. However, the complete solution of their equations would be a formidable task.

In a previous paper,[9] we demonstrated that the same physical content (i.e., explicit transverse momentum in the jet-calculus equations) could be obtained in so-called "backward-moving" Altarelli-Parisi equations, in which the mass of the partons evolves down (much as it does in Monte Carlo models). In this paper, we present results of the numerical solution of the equations and discuss the limitations of this approach.

Because our equations are simpler than the forward-moving BCM equations, we do not need to make the $x\to 1$ approximation. We solve the exact equations in moment space for a number of impact parameters. Inversion of the moments then leads to results in x space. Our answers agree with those of BCM for $x\to 1$ as expected; at lower x (where BCM's formula is not expected to be accurate), our results are more sharply peaked in impact parameter.

Inversion of the Fourier transform between impact parameter b and transverse momentum $p_\perp$ presents more problems. Nevertheless, we believe we can calculate this well enough to discern qualitative trends.

The outline of the paper proceeds along these lines. In Sec. II we explain the method we used in impact-parameter space to obtain values for moments of the nonsinglet quark propagator (i.e., the fragmentation function of quarks into the nonsinglet combination of quarks). These are compared with the explicit formula given by BCM, using their $x\to 1$ approximation. The inversion to transverse momentum introduces additional uncertainties, and hence it is discussed separately in Sec. III. Despite systematic problems due to the inversion, some trends remain. Relations with similar trends in the data are explored. Finally, Sec. IV contains a summary and conclusions.

 ©1986 The American Physical Society

II. THE VIEW FROM IMPACT-PARAMETER SPACE

A. Basic equations and methods

In this paper we focus on the equation for the nonsinglet quark propagator $\mathscr{D}^{\rm NS}(p_\perp,x)$ [see Eq. (2.1) of Ref. 8]

$$-k^2\frac{d}{dk^2}\mathscr{D}^{\rm NS}(Q^2,k^2;\mathbf{p}_\perp,x) = \int_x^1 \frac{\alpha(k^2z(1-z))}{2\pi}\frac{dz}{z^3}P_q^{qg}(z) \times\int\frac{d^2\mathbf{q}_\perp}{\pi}\delta(q_\perp{}^2-k^2g(z)) \times\mathscr{D}^{\rm NS}\left[Q^2,k^2;\frac{\mathbf{p}_\perp-\mathbf{q}_\perp}{z},\frac{x}{z}\right]. \quad (2.1)$$

After taking moments, and Fourier transforming in transverse momentum, we get

$$-k^2\frac{d}{dk^2}\tilde{\mathscr{D}}^{\rm NS}(Q^2,k^2;\mathbf{b};n) = \int_0^1\frac{\alpha(k^2z(1-z))}{2\pi}dz\,z^nP_q^{qg}(z) \times\int dq_\perp{}^2J_0(bq_\perp)\delta(q_\perp{}^2-k^2g(z)) \times\tilde{\mathscr{D}}^{\rm NS}(Q^2,k^2;z\mathbf{b};n)\,. \quad (2.2)$$

If we use the standard

$$g(z)=z(1-z),\quad \alpha(t)=\frac{1}{B\ln(t/\Lambda^2)},\quad B=\frac{11N_c-2N_f}{12\pi},$$

this becomes

$$-k^2\frac{d}{dk^2}\tilde{\mathscr{D}}(Q^2,k^2;\mathbf{b};n) = -\tilde{\mathscr{D}}(Q^2,k^2;\mathbf{b};n)\frac{C_F}{2\pi}\left[-\frac{3}{2}\alpha(k^2)+\frac{1}{B}\ln\left[\frac{\ln(k^2/\Lambda^2)}{\ln(Q_0{}^2/\Lambda^2)}\right]\right] + \int_0^1 dz\frac{\alpha(k^2z(1-z))}{2\pi}z^nC_F\left[\frac{1+z^2}{1-z}\right]J_0(bk[z(1-z)]^{1/2})\tilde{\mathscr{D}}(Q^2,k^2;z\mathbf{b};n)\,. \quad (2.3)$$

Our task is thus to solve this equation as a function of moment n and impact-parameter b, and then to invert back to longitudinal-momentum x and transverse-momentum p_t.

Because the right-hand side depends only on impact-parameter values $z\mathbf{b}$ smaller than those on the left-hand side, we set up a grid in impact-parameter space. The right-hand-side contributions $\mathscr{D}(zb)$ are then expressed in terms of the values $\mathscr{D}(b_i)$ on a grid, using a polynomial interpolation. We then solve simultaneously for the values $\mathscr{D}(b_i)$ using Runge-Kutta integration for the differential equations (in practice the standard package RKF45 was used). See the Appendix for some detailed comments on the solutions.

At this point, the choice of grid points b_i must be made. Choice of these depends to a great extent on the method one plans to use to invert the Fourier transform into transverse-momentum space. For reasons discussed below, we have used mainly the Gauss-Laguerre integration points in b^2.

B. Results and comparison with others

We have had some difficulties in solving for b^2 larger than 20 GeV^{-2}. (We use $\Lambda=0.2$ GeV, $Q_0{}^2=0.062$ GeV^2 to set the scale.) In particular, although the equations for the individual moments (2.2) can be solved at large b, we have been unable to obtain results accurate enough to allow reliable inversion of the moments to obtain values of $\mathscr{D}(b^2,x)$, using the Legendre-inversion method. Detailed comparison of various methods of moment inversion is provided in Ref. 10. As discussed there, the Legendre method is the most reliable technique for moment inversion; however, it is extremely sensitive to errors in the input moments. Our differential equation solutions produce large moments which are good to one part in 10^6, but the smallest moments have errors of about 1 part in 10^4. Since the results of the moment inversion must still be processed to invert from impact-parameter to transverse-momentum space, we desire the high accuracy which the Legendre technique can provide. Hence we limit ourselves here to the description of results in the (relatively) low b^2 region.

A measure of the accuracy of the method is obtained by determining whether the values got using 6 Gauss points in b agree with those using 7 Gauss points in b. On the whole, they do, showing that the method is reliable unless the values of the function being computed are too small. However, we have had difficulty going to 9 Gauss points—the errors in the solution of our integrodifferential equation are apparently large enough to cause problems with the Legendre-inversion technique.

For purposes of comparison, we use the formula

$$\mathscr{D}^{\rm NS}(Q^2,\mathbf{p}_\perp,Q)=D^{\rm NS}(Q^2,x)\int_0^\infty\frac{b\,db}{2\pi}J_0(bp_\perp)\exp\left[-\frac{C_F}{\pi}\int_{Q_0{}^2}^{Q^2}\frac{dk^2}{k^2}\alpha(k^2)\int_0^{k^2b^2x^2}\frac{dq^2}{q^2}[1-J_0(q)]\right] \quad (2.4)$$

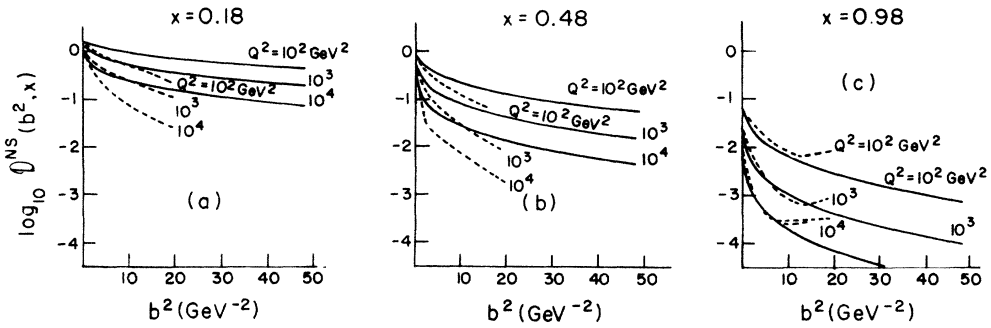

FIG. 1. Results in impact-parameter space for our calculation (dashed curves) and the BCM formula (solid curves). The two versions of our results used b^2 values for, respectively, six- and seven-point Gaussian Laguerre integration. The agreement of the two sets of answers for most cases shows that the solution of the differential equations provides results accurate enough for the Legendre inversion technique: (a) $x=0.18$; (b) $x=0.48$; (c) $x=0.98$.

given by BCM in their paper [Ref. 8, Eq. (C5)]. This was derived using the forward-moving Altarelli-Parisi equations with $p_\perp$ included; to get this simple formula they applied a rather brutal set of approximations which are good only for x near one.

Results at three sample values of x are displayed in Fig. 1, after the Legendre-moment inversion. To the extent that our equations have the same content as the BCM equations, as claimed in Ref. 9, we should then agree with their results near $x=1$. We see that this is indeed the case. At smaller x values, our results are more sharply peaked than theirs in impact parameter; thus we expect a broader distribution in transverse momentum.

As one might expect, the results are more sharply peaked in b^2 as q^2 grows, leading to distributions in $p_\perp$ which are broader as q^2 grows.

One question which has been raised in the recent experimental literature is the issue of whether the slope in $p_\perp$ changes monotonically with x.[6,7] To address this issue at the least confusing level, we show in Fig. 2 the overlay of the plots at various x values in impact-parameter space; of course the change of the slope in $p_\perp$ is inverse to the change of the slope in b^2 (see Fig. 6 below for the corresponding picture in transverse momentum).

III. RESULTS IN TRANSVERSE MOMENTUM

A. Methods and equations

Choice of the grid in b space depends to a great extent on the method one plans to use to invert the Fourier transform into transverse-momentum space. For instance, the method of Talman[11] requires values both at very small and rather large values of the impact parameter. Experimenting with various test functions led us to the conclusion that this method is inaccurate at large $p_\perp$ unless there are at least 16 input values for the function in impact-parameter space, and these input values are quite accurate.

We have found it difficult to solve Eq. (2.2) on a grid containing large b_i values in the sense that the smallest output answers seem to only be accurate to about 1 part in 10^4. While this might sound very good, it is not good enough to provide sensible answers after both x and b inversions are performed. Possibly our polynomial interpolation is a poor way to approximate the function between grid points, since it necessarily has incorrect behavior at large b.

In any case, we decided to focus instead on a method of

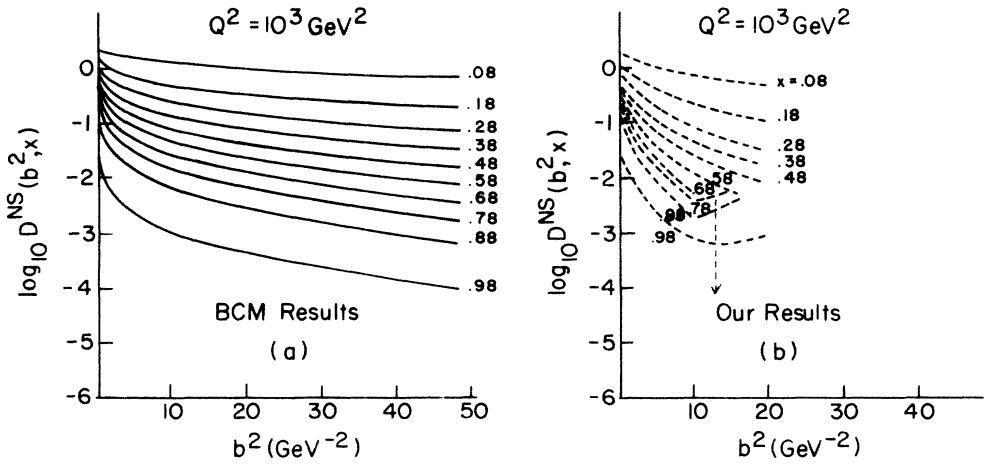

FIG. 2. Change with x of the results in b^2 at $Q^2=1000\ GeV^2$. (a) BCM results from Eq. (2.4); (b) our results.

inversion of the Fourier transform suggested by nuclear physicists[12] accustomed to using data for the transverse-momentum distribution in electron scattering to yield charge-density profiles for nuclei. In this technique, the data is expanded in a series of Laguerre polynomials:

$$f(b^2)=\sum_{n=0}^{N-1} e^{-(\alpha/2)b^2} A_n L_n\left[\frac{\beta}{2}b^2\right] . \tag{3.1}$$

These have the remarkable property that their Fourier transform is exactly known:[13]

$$\int_0^\infty J_0(xy)e^{-(\alpha/2)x^2}L_n\left[\frac{\beta}{2}x^2\right]x\,dx = \frac{(\alpha-\beta)^n}{\alpha^{n+1}}e^{-y^2/2\alpha}L_n\left[\frac{\beta y^2}{2\alpha(\beta-\alpha)}\right] . \tag{3.2}$$

Hence the transform of the series will yield a formula which can be evaluated at any $p_\perp$ desired.

In order to facilitate this expansion in Laguerre polynomials, we choose our evaluation points b_i to be exactly the Gauss-Laguerre points for N-point integration. Then the coefficients in the series are

$$A_n=\int_0^\infty e^{-(2-\alpha)b^2/2}f(b^2)db^2 \approx \sum_{i=1}^{N} e^{-(\beta-\alpha)b_i^2/2}f(b_i^2)w(i) \tag{3.3}$$

[here we have picked $\beta=2$ in Eq. (3.2) in order to use the Gauss points, and the weights $w(i)$ include the usual exponential factor].

We have one feature which is different from the nuclear physicists—we know the value at $b=0$ as well as the value at the other Gauss points. In fact, we know this value best of all because this is the usual QCD result obtained from the Altarelli-Parisi equations—the integral over all transverse momentum. In order to incorporate this into our scheme, we fit the parameter α in order to make our series approximate this value as closely as possible. The A_n are functions of α, as shown in (3.3). Choosing a value for α then defines all constants in Eq. (3.1).

B. Results and comparison with others

Our results in transverse momentum are immediately given by

$$f(p_\perp^2)=\sum_{n=0}^{N-1} e^{-p_\perp^2/2\alpha}\frac{A_n}{\alpha}\left[\frac{\alpha-2}{\alpha}\right]^n L_n\left[\frac{p_\perp^2}{\alpha(2-\alpha)}\right] . \tag{3.4}$$

Sample values are shown in Fig. 3. As expected, we agree with the BCM results at large x, and our $p_\perp$ distributions are somewhat broader at small x.

One disturbing aspect of the results in Fig. 3 is the large oscillations. Actually, as can be seen from Fig. 4 where the same results are shown on a linear scale, these oscillations are not nearly as dramatic as they appear on the logarithmic graph. Nevertheless, they make it difficult to compare our results with BCM; and we suspect that these oscillations are not real, but artifacts of the method used.

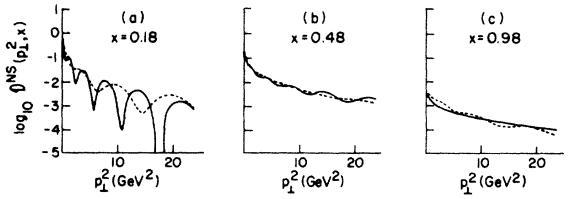

FIG. 3. Plots of Eq. (3.4) at $Q^2=1000$ GeV^2. Solid curve is from BCM Eq. (C5); dashed curve shows our result.

(The location of the dips changes if a different number of Laguerre polynomials is used in the initial expansion.)

A method of overcoming this is to average the results over some region in $p_\perp$. This can be done very easily using the convolution theorem, since

$$f_1(\mathbf{b})f_2(\mathbf{b})$$

is the Fourier transform of

$$\int \tilde{f}_1(\mathbf{p}'-\mathbf{p})\tilde{f}_2(\mathbf{p}')d^2\mathbf{p}' .$$

Hence, if we multiply our results in b space by the Gaussian

$$e^{-(A/2)b^2}$$

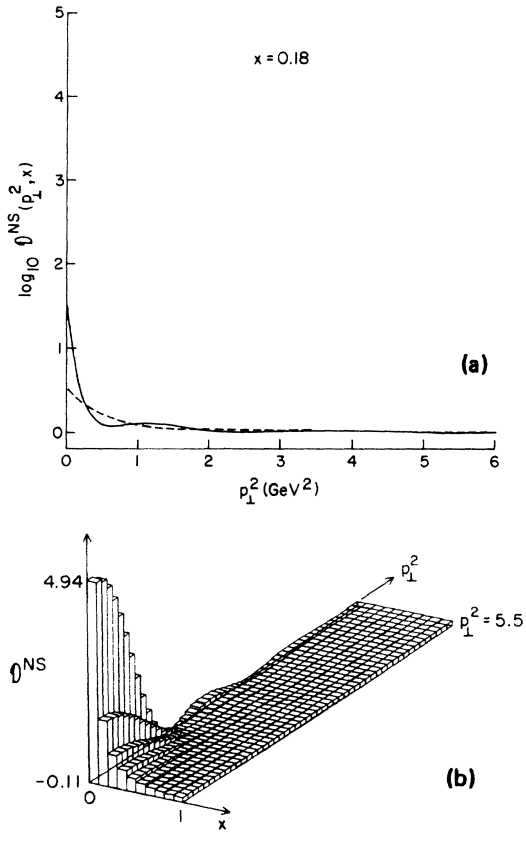

FIG. 4. (a) Figure 3(a) plotted on a linear scale, showing that the results of the Fourier transform in fact do not oscillate much on an absolute basis; (b) BCM results on linear scale, showing x and $p_\perp^2$ dependence.

we achieve an average of the $p_\perp$ results over neighboring values, which should smear out some of these dips.[14]

We display in Fig. 5 the results of multiplying by $e^{-0.05b^2/2}$, and $e^{-0.15b^2/2}$, which have the effect of averaging over nearby $p_\perp$ within 0.3 and 0.45 GeV, respectively, of the "observed" value. Note that the results at large x are not very much affected by the averaging.

We now wish to compare with data. Ideally we would like to use data containing only the nonsinglet-quark-fragmentation function. There are a number of experimental distributions which select this particular case, which picks out the "incident" quark from the spray (as opposed to quarks produced in pairs by the QCD branching).

For instance, at typical center-of-mass energies for e^+e^- collisions, the jet masses are not large enough to allow creation of charm-anticharm pairs. Hence all the charmed particles that are seen come from the quarks which originated the jet.[15] Data exist for the x and $p_\perp$ distribution of these charmed particles; however, to date it has been presented only as a function of either x (Ref. 16) or $p_\perp$ (Ref. 17). We have been unable to find a presentation which shows the x dependence of the $p_\perp$ slope.

Other similar cases involve the difference between π^+ and π^- distributions in charged-current neutrino and antineutrino scattering off protons. Reactions in which a W^- strikes the proton create jets of d quarks or $\bar{u}$ quarks. These will produce *leading* π^- particles; all the π^+ mesons and all the other π^- mesons will come from radiation off the quark. Hence the difference between π^- and π^+ distributions tells us about the leading quark and hence the nonsinglet distribution. Exactly the same reasoning applies to the W^+. Data are available on these pion distributions;[18] again the presentation does not allow us to see the x variation of the transverse-momentum slope.

Finally, the fragmentation functions of the u quark into both signs of charged pions have also been determined,[19] and the difference of these is another measure of the fragmentation into the nonsinglet combination of quarks. Again the best quantity for comparison with our calculations, the x dependence of the $p_\perp$ slope of the difference between the π^+ and π^- fragmentation functions, is not shown. In Ref. 20, however, the same collaboration (EMC) does examine some aspects of the x and $p_\perp$ correlations. In particular, Fig. 2 of Ref. 20 shows that at large x (z in their notation) the average value of $p_\perp$ is lower for lower values of Q^2. This is similar to the $p_\perp$ flattening observed in our Fig. 7 for large Q at large x.

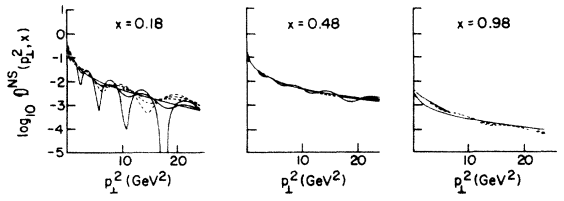

FIG. 5. Consequences of smoothing at $Q^2=1000$ GeV^2, showing the results of multiplying the impact-parameter results by 1, $e^{-0.05b^2/2}$ and $e^{-0.15b^2/2}$. BCM results are solid curve; our results are dashed curve. We believe this smoothing preserves the essential physics results while removing artifact dips from our approximate Fourier inversion method.

Although various aspects of these distributions have been measured, the data do not seem to have been presented in exactly the form we would like for easy comparison with our results. In particular, data showing the $p_\perp$ behavior for various x bins, or vice versa, are not given in the literature. No doubt this is because statistics are limited in many cases, and hence not adequate for double binning. We look forward to having such detailed information available in the future.

Experimental information on the interrelation of transverse and longitudinal momentum does exist for more general distributions. In order to see whether our results are even qualitatively reasonable, we will compare them with these (always remembering that other terms may enter).

Because we do not wish to obscure the basic QCD results we have calculated, we do not multiply by phenomenological fragmentation functions into pions, kaons, protons, etc. This means that our comparison with data must be qualitative. However, since the hadronization functions are expected to introduce only small additional $p_\perp$ (of the order of 200 MeV), it is sensible to compare with data those trends which can be observed at the GeV level in $p_\perp$.

In Fig. 6 we show how the slope in $p_\perp$ changes with x.

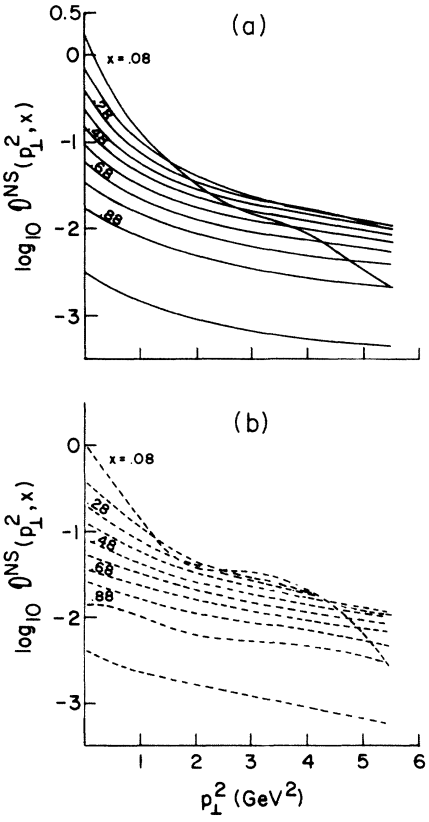

FIG. 6. Slope in $p_\perp{}^2$ as a function of x at $Q^2=1000$ GeV^2, using a smoothing function $e(-0.1b^2/2)$ in impact-parameter space: (a) BCM results; (b) our results.

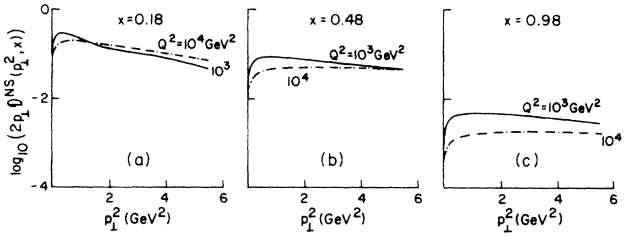

FIG. 7. Behavior of $2p_\perp \mathcal{D}(p_\perp{}^2,x)$ at various x values as a function of Q^2. Note that the distributions become broader as Q^2 rises. Because the Altarelli-Parisi equations damp large x as Q^2 increases, the crossover point tends to move to larger $p_\perp$ as x increases. Both contributions have been multiplied by the smoothing function $e(-0.1b^2/2)$ in impact-parameter space prior to the inversion.

On the whole, distributions become broader as x increases until x gets to about 0.7, after which the slope seems rather constant with x. The increase in $\langle p_\perp \rangle$ at small x agrees with the data presented in Fig. 34 of Ref. 6; however we do not obviously have the decrease in $\langle p_\perp \rangle$ at very large x shown in the data. Our "flattening off" of $\langle p_\perp \rangle$ at large x is more like the data presented in Fig. 26 of Ref. 7.

In Fig. 7 we show the transverse-momentum behavior at various x values for two different values of Q^2. Notice that the distributions become broader as Q^2 increases, as expected (see Fig. 31 of Ref. 6), and that the "crossover" point appears at larger and larger transverse momentum as x increases.

Similar results are presented in Fig. 8, using the "scaling" variable $x_T=2p_\perp/W$. This is to be compared with Fig. 42 of Ref. 6, which is integrated over all x. The data and the predictions show the same hierarchy: low Q^2 is lowest at small x_T, but largest at large x_T. Note that we have used rather large "smoothing" coefficients here, especially for $Q^2=10^4$ GeV^2 (where a very large range of $p_\perp$ is needed to explore this region of x_T); our results are therefore more qualitative than quantitative.

Both Figs. 7 and 8 are rather flatter in transverse momentum than the corresponding distributions in the data. This is due to underpopulation of the region at small $p_\perp$. Our results are somewhat similar to those presented in Fig. 14 of the KUV paper (Ref. 3). Since the data include results of the other $\mathcal{D}$ functions as well as the nonsinglet ones, we cannot at this point tell whether the discrepancy is due simply to the other contributions, or whether nonperturbative effects need to be invoked. It is clear that the nonsinglet distribution is rather special, since it involves only the incident quark in the jet and has less singular behavior at $x=0$ than the other contributions. These other pieces, thus, tend to be large at small x and to affect the overall size of the results. Assuming that they also have the feature that small x is peaked more sharply in transverse momentum (shown for the nonsinglet case in Fig. 7), they will contribute to an overall enhancement of the cross section at small $p_\perp$, in the direction of agreement with the data.

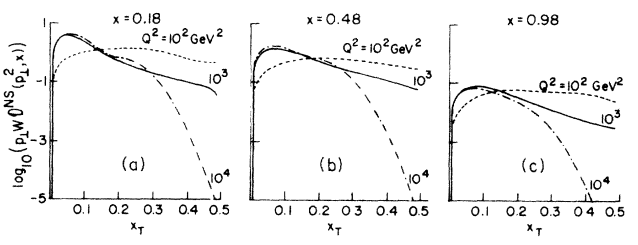

FIG. 8. Same as Fig. 7 except that the parameter used is the "scaled" variable $x_T=2p_\perp/W$. Because of the wide range of $p_\perp$ used, substantial smoothing factors were necessary in some cases. The results plotted use $e^{Ab^2/2}$ with $A=0.7$ at $Q^2=100$ GeV^2, $A=0.4$ at $Q^2=1000$ GeV^2, $A=8$ at $Q^2=10\,000$ GeV^2.

IV. SUMMARY AND CONCLUSIONS

By solving explicitly the backward-moving Altarelli-Parisi equations suggested in an earlier paper, we have tested their usefulness as a means for studying the transverse-momentum properties of jets. Results agree with previous solutions by BCM of the forward-moving equations containing transverse momentum, in the region near $x=1$, where the previous solution was expected to be valid. At smaller x values, our results are broader in $p_\perp$ than BCM's approximate formula.

We obtain an increase of $\langle p_\perp \rangle$ with x at small x similar to that seen in jet data. The Q^2 variation of behavior in $p_\perp$ and x_T $(=2p_\perp/Q)$ is also similar to that in the data. More detailed comparison with experimental results would require computation of $\mathcal{D}$ functions other than the nonsinglet; and the inclusion of phenomenological fragmentation functions; however, it is expected that these additions would improve the agreement.

The programs which perform these computations can be run in a finite time on the CYBER 175; time to integrate the equations varies, of course, with the Q^2 considered, but the results shown in impact-parameter space typically required less than 80 CPU seconds to compute the values at 7 grid points plus $b=0$. Another moderately time-consuming calculation is the fit of the parameter α in the Laguerre expansion used for the Fourier-transform inversion. On the whole, this is not much by modern computing standards and, if one were so inclined, the programs could no doubt be improved to increase both speed and accuracy.

Our solutions of the integrodifferential equation for *moments in impact-parameter space* are quite accurate and reproducible. Further calculations by the differential-equations approach (such as solution of the remaining equations in Ref. 9) await a more reliable method of inversion from impact parameter to transverse momentum. In other words, the *full* numerical consequences of the backward-moving equations can be achieved either by resolving the above difficulty, or by solving the integrodifferential equations directly in x and $p_\perp$ space. This sort of calculation may become commonplace as supercomputers are used more frequently with large meshes in integral equations, but for the moment the physics gains do not seem to warrant the programming difficulties.

Thus, if we stick with computations of manageable size, further calculations by the differential-equations approach

are not likely to yield as much new information as the QCD Monte Carlo approach. In addition to the difficulties mentioned above, incorporation of extra degrees of freedom into the differential equations increases the complexity of the solution process a great deal, whereas the Monte Carlo has all these kinematic variables to begin with.

ACKNOWLEDGMENTS

This work was supported in part by the U.S. Department of Energy under Contract No. DEACO 276 ERO 1195 (L.M.J.), NATO Research Grant No. 779/83 (L.M.J.) and (R.M.), Natural Sciences and Engineering Research Council (Canada) Operating Grant No. A8070 (R.M.), and Natural Sciences and Engineering Research Council International Collaborative Research Grants (R.M.). L.M.J. would like to thank the Natural Sciences and Engineering Research Council, and L.S. the University of Illinois at Urbana-Champaign Physics Department for financial support. We would like to thank the University of Illinois Research Board for a contribution of computer time. In addition, we would like to acknowledge helpful conversations with a large number of colleagues, in addition to those mentioned specifically in the references. These include R. Schult, J. D. Talman, B. Crespi, C-K. Ng, H. W. Wyld, L. Opsahl, K. S. Sowmya Narayanan, and Dmitry Krass. We thank Paul Nakroshis for preparing Fig. 4(b).

APPENDIX

In this appendix we discuss a few of the more detailed points in the evaluation of the expression in Eq. (2.3). In particular, after a polynomial approximation is made for $\mathscr{D}(zb)$, the z integral reduces to terms of the form

$$\mathscr{A}_p(b_j,k)=\int_0^1 dz\, z^P J_0(b;k[z(1-z)]^{1/2}) \equiv A_p\left[\frac{b_j k}{2}\right] \tag{A1}$$

and

$$\mathscr{I}(b_j,k)=\int_{p_0{}^2}^{k^2}\frac{dt}{t}\alpha(t)J_0(b_j\sqrt{t}) = \left[\int_{Q_0{}^2}^{Q^2}-\int_{k^2}^{Q^2}\right]\frac{dt}{t}\alpha(t)J_0(b_j\sqrt{t}) . \tag{A2}$$

The $\mathscr{I}$ functions can, as shown, be split into two terms. One ($\int_{Q_0{}^2}^{Q^2}$) is evaluated once for each Q^2 and b_i, and the other ($\int_{k^2}^{Q^2}$) is evaluated as a separate variable in the Runge-Kutta integration.

However, the $\mathscr{A}_p$ function in Eq. (A1) would be rather time consuming to evaluate at each step of the integrator. In fact, these can be obtained analytically beginning from Eq. (29) of Ref. 21.

$$\int_0^a \frac{x}{(a^2-x^2)^{1/2}}\cos[\beta(a^2-x^2)^{1/2}]J_0(x)dx = \frac{1}{(\beta^2+1)^{1/2}}\sin[a(\beta^2+1)^{1/2}] . \tag{A3}$$

Hence, setting $\beta=0$, we find by standard methods ($x=bk/2$)

$$\mathscr{A}_0(b,k)=A_0\left[\frac{bk}{2}\right]=\frac{\sin x}{x} ,$$
$$A_1(x)=\frac{1}{2}\frac{\sin x}{x} , \tag{A4}$$
$$A_2(x)=\frac{1}{4}\left[\frac{\sin x}{x}-\frac{\cos x}{x^2}+\frac{\sin x}{x^3}\right] .$$

Using Bessel's equation for J_0, these integrals obey the recursion relations ($x=bk/2$)

$$A_{p+2}(x)=\frac{1}{4}(p+1)\left[2A_{p+1}(x)\left[\frac{1}{p}+\frac{1}{p+1}\right]-\frac{1}{p}A_p(x) + \frac{1}{x^2}[(p+1)A_p(x)-pA_{p-1}(x)]\right] \tag{A5}$$

Hence all the necessary ones can be generated from simple functions.

Unfortunately the recursion relation runs into difficulties when k is small. In this case, we use a series approximation, which is also quickly evaluated.

[1]J. Ellis, M. K. Gaillard, and G. G. Ross, Nucl. Phys. **B111**, 253 (1976).
[2]G. Sterman and S. Weinberg, Phys. Rev. Lett. **39**, 1436 (1977).
[3]K. Konishi, A. Ukawa, and G. Veneziano, Nucl. Phys. **B157**, 45 (1979).
[4]G. Curci, M. Greco, and Y. Srivastava, Nucl. Phys. **B159**, 451 (1979); R. K. Ellis and R. Petronzio, Phys. Lett. **80B**, 244 (1979).
[5]R. Hollebeek, in *Proceedings of the 1981 International Symposium on Lepton and Photon Interactions at High Energies, Bonn,* edited by W. Pfeil (Physikalisches Institut, Universität Bonn, Bonn, 1981), p. 1.
[6]M. Althoff *et al.*, Z. Phys. **22**, 307 (1984).
[7]D. Bender *et al.*, Phys. Rev. D **31**, 1 (1985).
[8]A. Bassetto, M. Ciafaloni, and G. Marchesini, Nucl. Phys. **B163**, 477 (1980).
[9]L. M. Jones and R. Migneron, Phys. Rev. D **30**, 560 (1984); see also *Proceedings of the XXII International Conference on High Energy Physics, Leipzig, 1984,* edited by A. Meyer and E. Wieczorek (Academie der Wissenschaften der DDR, Zeuthen, DDR, 1984), Vol. I, p. 286.
[10]L. M. Jones and L. R. Opsahl, J. Phys. G (to be published).
[11]J. D. Talman, J. Comput. Phys. **29**, 35 (1978).
[12]We thank D. G. Ravenhall and J. Wambach for their tutelage;

they share no blame for problems with the results.

[13]A. Erdélyi *et al.*, *Tables of Integral Transforms* (Bateman Manuscript Project), edited by A. Erdélyi *et al.* (McGraw-Hill, New York, 1954), Vol. 2, p. 13.

[14]We thank Michael Stone for reminding us of this application of the convolution theorem.

[15]Of course for the case of the charmed quark, we need to adjust the Q_0 in the integration to allow for the larger mass. This is not a problem. See, for instance, L. M. Jones, Phys. Rev. D **28**, 236 (1983).

[16]S. Ahlen *et al.*, Phys. Rev. Lett. **51**, 1147 (1983).

[17]M. Althoff *et al.*, Phys. Lett. **135**, 243 (1984).

[18]N. Schmitz, in *Proceedings of the 1981 International Symposium on Lepton and Photon Interactions at High Energies, Bonn* (Ref. 5), p. 527.

[19]J. J. Aubert *et al.*, Phys. Lett. **160B**, 417 (1985).

[20]J. J. Aubert *et al.*, Report No. CERN-EP/85-72 (unpublished).

[21]A. Erdélyi *et al.* (Ref. 13), p. 337.